Research Paper
J. Astron. Space Sci. 40(4), 237-245 (2023)
https://doi.org/10.5140/JASS.2023.40.4.237

JASS Journal of Astronomy and Space Sciences

Analysis of Tip/Tilt Compensation of Beam Wandering for Space Laser Communication

Seok-Min Song[1,2], Hyung-Chul Lim[1†], Mansoo Choi[1], Yu Yi[2]

[1]Korea Astronomy and Space Science Institute, Daejeon 34055, Korea
[2]Department of Astronomy and Space Science, Chungnam National University, Daejeon 34134, Korea

Laser communication has been considered as a novel method for earth observation satellites with generation of high data volume. It offers faster data transmission speeds compared to conventional radio frequency (RF) communication due to the short wavelength and narrow beam divergence. However, laser beams are refracted due to atmospheric turbulence between the ground and the satellite. Refracted laser beams, upon reaching the receiver, result in angle-of-arrival (AoA) fluctuation, inducing image dancing and wavefront distortion. These phenomena hinder signal acquisition and lead to signal loss in the course of laser communication. So, precise alignment between the transmitter and receiver is essential to guarantee effective and reliable laser communication, which is achieved by pointing, acquisition, and tracking (PAT) system. In this study, we simulate the effectiveness of tip/tilt compensation for more efficient laser communication in the satellite-ground downlink. By compensating for low-order terms using tip/tilt mirror, we verify the alleviation of AoA fluctuations under both weak and strong atmospheric turbulence conditions. And the performance of tip/tilt correction is analyzed in terms of the AoA fluctuation and collected power on the detector.

Keywords: satellite optical communication, downlink laser, low-order adaptive optics, tip/tilt compensation

1. INTRODUCTION

The role of lasers in the utilization of space is gaining prominence in today's context. Lasers can enable various applications such as satellite laser ranging (SLR) and laser communication. Laser communication, in particular, offers faster data transmission speeds compared to traditional RF communication methods, features a smaller beam footprint and enhanced security, and is characterized by a reduced size, weight, and power (SWaP) profile. As a result, it is being considered as a potential replacement for RF communication in future space communication. However, unlike RF communication, laser communication necessitates precise directional operations between the satellite and the ground station, namely PAT (Abdelfatah et al. 2022). During the PAT operations, atmospheric effects, present between the ground and space, inevitably cannot be excluded when performing coarse acquisition. Consequently, various studies have been carried out to correct for atmospheric effects in order to maximize the effectiveness of space lasers from the ground (Tyson 1996; Yang et al. 2006; Shamsipour et al. 2018).

To correct for these atmospheric effects, an adaptive optics system is required. The simplest form of adaptive optics is tip/tilt correction, which is akin to correcting the tilt of the wavefront in two dimensions. In this type of adaptive optics, the tip/tilt mirror is an important component. It is installed in the optical path, and by tilting the mirror, it corrects distorted beams, particularly with the inclusion of a fast steering mirror (FSM). By compensating for optical axis misalignment, it prevents image degradation, retains the intensity of the target source, and maintains optical characteristics. Many of the aberrations induced by the atmosphere can be

Received 06 OCT 2023 **Revised** 07 NOV 2023 **Accepted** 12 NOV 2023
†**Corresponding Author**
Tel: +82-42-865-3235, E-mail: hclim@kasi.re.kr
ORCID: https://orcid.org/0000-0001-5266-1335

mitigated using this approach. Additionally, it not only is cost-effective but also provides a low SWaP in terms of the design engineering. Therefore, we utilize an adaptive optics system employing tip/tilt correction to mitigate the atmospheric turbulence. In addition, various factors such as satellite orbit, communication modulation, transmitter beam performance, and receiving aperture can affect the downlink channel performance in turbulent conditions (Lim et al. 2020a, b). However, to assess the effect of tip/tilt correction, we keep the impact of other factors fixed.

We are planning to establish a ground station for future laser communication with satellites. This ground station will utilize the existing infrastructure of the GEOL station (at Geochang, Korea; Lim et al. 2018), which is currently used for SLR, with the goal of constructing a PAT system for laser communication. In this paper, we simulate the angle-of-arrival (AoA) fluctuation caused by atmospheric turbulence for the purpose of building the ground station. We also analyze the intensity fluctuation of the beam detected by the detector. Furthermore, we present the effects of coarse acquisition based on the results obtained using tip/tilt mirrors. It is important to note that the results we present focus solely on scintillation due to pointing error and are intended to verify the correction effects of tip/tilt compensation.

2. METHODS

2.1 System Configuration

Our simulation utilizes the infrastructure of the GEOL SLR station. We employ a 1m telescope and use a laser with a signal wavelength of λ = 1,550 nm for laser communication. Additionally, we introduce a beacon beam to measure atmospheric effects, assuming that it resolves the isoplanatism angle issue resulting from different propagation paths compared to the signal beam, as seen in conventional applications such as laser guide stars. Table 1 provides details of the parameters for the proposed system.

Table 1. System configuration parameters

	Parameter	Symbol	Value
Receiver (telescope)	Telescope aperture (radius)	$D(R)$	1 m (0.5 m)
	Focal length	f	1.5 m
	Tracking & pointing accuracy		~1 arcsec
Detector (photodiode)	Detector radius	a	37.5 μm
	Responsivity	R_D	1 A/W
	Sampling frequency	f_s	≤ 150 kHz
Tip/tilt mirror	Closed-loop bandwidth	f_c	≤ 850 Hz
Transmitter (satellite)	Communication signal wavelength	λ	1,550 nm
	Satellite altitude	H	300 km

2.2 Refractive-Index Structure Parameter

Due to temperature gradients in the atmosphere, turbulent spatial fluctuations cause refraction of the laser propagation direction, simultaneously affecting the wavefront phase. The refractive index structure parameter, known as C_n^2, characterizes the refractivity of atmospheric turbulence, which is also referred to as optical turbulence. Numerous models for representing this parameter have been developed. In our research, we employ the Hufnagel-Valley (H–V) model, which is expressed as follows (Andrews, 2019):

$$C_n^2(h) = 0.00594\left(\frac{w}{27}\right)^2 \left(10^{-5}h\right)^{10} \cdot exp\left(-\frac{h}{1{,}000}\right) + 2.7\cdot 10^{-16}\cdot exp\left(-\frac{h}{1{,}500}\right) + A\cdot exp(-h/100) \quad (1)$$

where w is root-mean-square(rms) wind speed in m/s, A is the nominal value of $C_n^2(0)$ at the ground in $m^{-2/3}$, and h is the height above sea level in m.

As evident from this model, the refractive-index structure profile with respect to altitude is determined by the values of w and A, which can be considered as a measure of turbulence strength. In this paper, we consider the profile known as the H–$V_{5/7}$ model (w = 21 m/s, $A = 1.7\times10^{-14}$ $m^{-2/3}$) for weak turbulence and substitute w = 32 m/s, $A = 3.0\times10^{-13}$ $m^{-2/3}$ into the H–V model for strong turbulence. Fig. 1 depicts the refractive index values at different altitudes calculated based on the conditions determined above for both weak and strong turbulence.

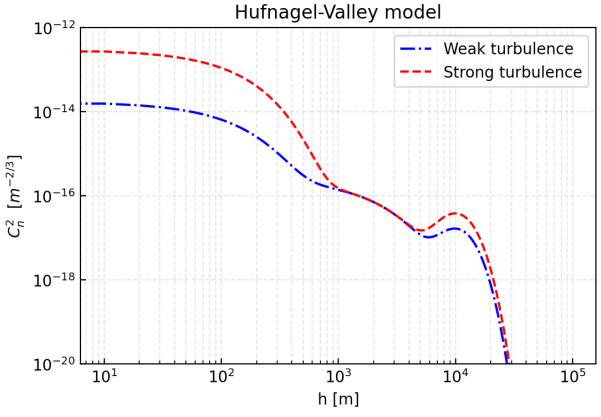

Fig. 1. C_n^2 model profiles according to height for each strong (red) and weak (blue) turbulence.

2.3 Angle-of-Arrival (AoA) Fluctuation

The wavefront of the laser beam arriving at the receiver is distorted and refracted due to atmospheric turbulence, ultimately reaching the receiver. This causes the beam's center to deviate from the on-axis at the receiver's focal plane, resulting in spot motion. In addition, jitter from both the transmitter (satellite) and the receiver (ground station) contributes to image dancing. These effects are referred to as AoA fluctuations and occur randomly depending on turbulent conditions. The variance of random AoA fluctuations is denoted as $\langle \beta_a^2 \rangle$ and can be expressed as follows (Andrews & Phillips, 2005):

$$\langle \beta_a^2 \rangle = 2.91 sec\zeta \left(\int_{h_0}^{H} C_n^2(h) dh \right) D^{-1/3} \tag{2}$$

where ζ is the zenith angle and D is the receiver's (telescope) aperture diameter.

In this case, the AoA fluctuation results in the displacement from the center at the focal plane. The variance of this displacement is expressed Eq. (3) as rms (Fernandez et al. 2018), and it is known to follow a Rayleigh distribution.

$$\sqrt{\langle r_a^2 \rangle} = f \cdot tan \sqrt{\langle \beta_a^2 \rangle} \tag{3}$$

where, f is focal length of the receiver.

Fig. 2 illustrates how the center of the beam reaches the focal plane due to AoA fluctuations caused by atmospheric turbulence. The dashed black circles in each figure represent the area where the detector detects the beam. In the case of weak turbulence, most of the beam is concentrated within the detector's area and at its center. In contrast, for strong turbulence, the beam is more dispersed from the center and, in severe cases, it can be observed that it extends beyond the detector's area. Such errors from the center are one of the factors degrading the power collected by the detector, but they can be compensated for using a tip/tilt mirror.

2.4 Beam Spread on Focal Plane and Airy Disk Approximated in Gaussian Distribution

When a beam reaches the focal plane, it is well-known that

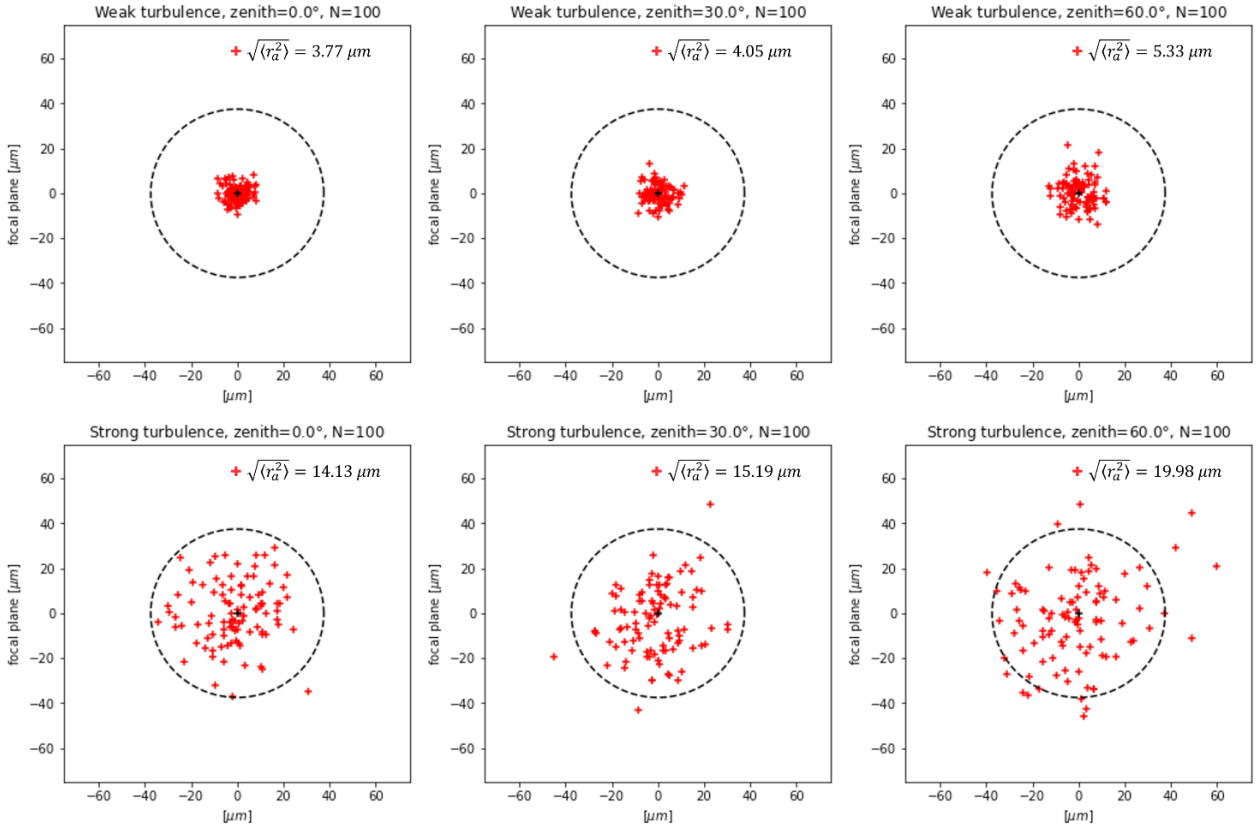

Fig. 2. The center of the beam reaching the focal plane varies with the zenith angle and the intensity of turbulence. The dashed black circles represent the area detectable by the detector.

the intensity of the beam follows a distribution called the Airy disk. As shown in Fig. 2, the center of the beam at the focal plane is offset from the center of the detector. The intensity of the beam that reaches the focal plane forms an Airy disk centered on the beam's center. As a result, a portion of the beam's intensity distribution extends beyond the area that the detector can capture. Only the portion of the beam within the detector's detectable area is received, allowing us to calculate the received beam's power. For the sake of convenience in our calculations, we approximated the beam's Airy disk distribution as a Gaussian distribution. The following equation can be used to approximate the Airy function as a Gaussian function (Cheon & Muschinski 2007; Fig. 3):

$$\underbrace{\left(\frac{2\mathcal{J}_1(x)}{x}\right)^2}_{\text{(Airy function)}} \approx \underbrace{\exp\left[-(0.5216\,x)^2\right]}_{\text{(Gaussian function)}} \tag{4}$$

where $\mathcal{J}_1(x)$ is the first-order Bessel function and $x = kR\sin\theta$ consisting of the wave number k, the aperture radius R, and the observation angle θ.

Furthermore, when the beam reaches the focal plane, it not only moves away from the center but also experiences spreading of intensity profile from the beam's center due to diffraction and turbulence. As shown in Fig. 4, atmospheric turbulence exacerbates this spreading, causing the radius of the beam reaching the focal plane to increase further. The full width half maximum (FWHM) of the beam due to diffraction and turbulence is expressed as follows:

$$FWHM_D = f\frac{\lambda}{D} \quad (\text{diffraction}-\text{induced}) \tag{5}$$

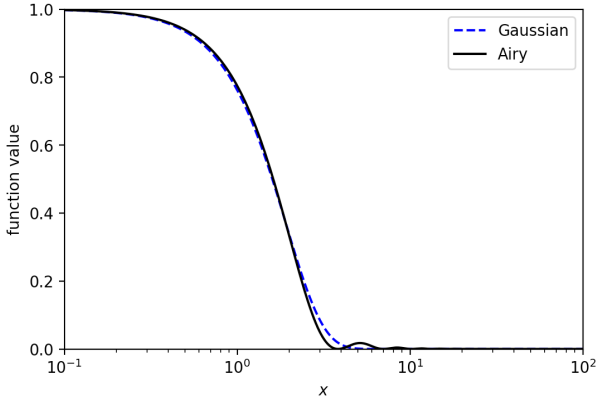

Fig. 3. Comparison of Airy function (black solid line) and approximated Gaussian function (blue dashed line).

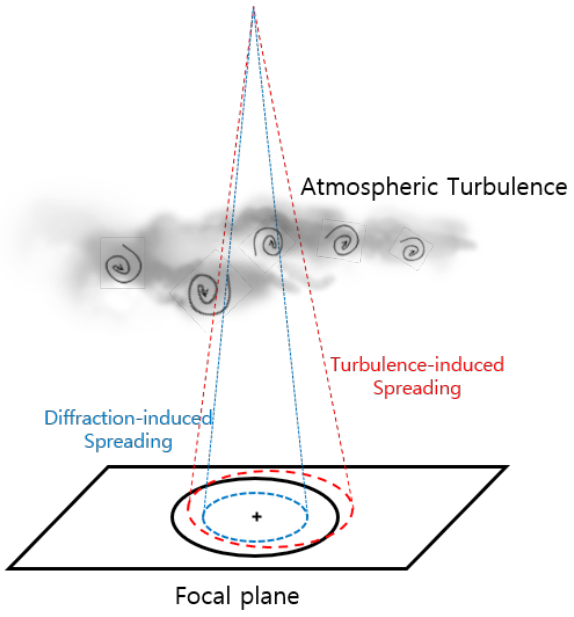

Fig. 4. Diagram of diffraction & turbulence -induced beam spreading.

$$FWHM_T = f\frac{\lambda}{r_0} \quad (\text{turbulence}-\text{induced}) \tag{6}$$

$$r_0 = 1.68\cdot k^{-6/5}\left(\sec\zeta\int_{h_0}^{H} C_n^2(h)\,dh\right)^{-3/5} \quad (\text{for downlink}) \tag{7}$$

The beam's FWHM due to turbulence is characterized through a metric known as the Fried parameter, denoted as r_0, which represents the optical system's ability to withstand the influence of atmospheric turbulence to some extent. The FWHM of the beam at the focal plane can be calculated by consolidating Eqs. (5) and (6) as follows (Robbe et al. 1997):

$$\begin{aligned} FWHM &= \sqrt{(FWHM_D)^2 + (FWHM_T)^2} \\ &= \frac{\lambda f}{D}\sqrt{1+\left(\frac{D}{r_0}\right)^2} \end{aligned} \tag{8}$$

However, in a Gaussian distribution beam profile, the FWHM represents the diameter at which the beam's intensity becomes 1/2 of its maximum intensity, which does not fully characterize the beam size. The beam radius corresponds to the point where the beam's intensity drops to $1/e^2$ of its maximum intensity. Using this relationship, we calculate the beam radius as follows:

$$\omega_{st} \cong FWHM \sqrt{\frac{1}{2ln2}} \tag{9}$$

In this way, we obtain a Gaussian distribution-approximated beam intensity profile through the beam radius, and this in turn allows us to calculate the power of the beam received by the detector. The results of these calculations are presented in Section 3.

2.5 Tip/Tilt Compensation

Several factors, including atmospheric turbulence-induced AoA fluctuation, contribute to the tilt error (σ_{tilt}). It can also be calculated through FSM control as follows (Olivier et al. 1993) :

$$\sigma_{tilt}^2 = \sigma_{SNR}^2 + \sigma_{TA}^2 + \sigma_{BW}^2 + \sigma_{HO}^2 \tag{10}$$

Here, σ_{SNR} arises due to the finite signal-to-noise ratio (SNR), and σ_{TA} is induced by finite angular separation between an astronomical object (or guide object) and a reference object, referred to as tilt anisoplanatism. σ_{BW} represents the error resulting from the finite closed-loop bandwidth of the tip/tilt compensation system while σ_{HO} denotes the error in the wavefront tilt estimate due to centroid anisoplanatism and uncorrected high-order aberrations expressible by Zernike polynomials. The tilt error before compensation is equivalent to the previously mentioned AoA fluctuation.

Looking at each of the errors, first, σ_{SNR} can be expressed as follows:

$$\sigma_{SNR} = \frac{3\pi}{16}\frac{1}{SNR}\frac{\lambda}{D}\sqrt{\left(\frac{2f_c}{f_s}\right)\tan^{-1}\left(\frac{f_s}{2f_c}\right)} \tag{11}$$

Here, f_c is the tip/tilt system's closed-loop bandwidth, and f_s is the sampling frequency. f_s should have a value faster than the tilt Greenwood frequency to track AoA fluctuations caused by atmospheric turbulence, and f_c should be at least four times the Greenwood frequency to design an appropriate adaptive optics system (Hemmati 2020).

σ_{TA} represents the error that occurs when using different optical paths, such as when employing a laser guide star or an astronomical object for atmospheric correction, that are distinct from the signal laser. In this study, using a beacon beam aligns with the same optical path as the signal beam, and therefore, σ_{TA} is considered to be 0.

σ_{BW} is the error that arises because the atmosphere changes during the finite time that the FSM's closed-loop corrects the wavefront tilt induced by the atmosphere. During this time, the object and the reference wavefront tilt change, leading to an error. This error is a dominant factor affecting the tip/tilt adaptive optics system.

$$\sigma_{BW} = \frac{f_T}{f_C}\frac{\lambda}{D} \tag{12}$$

$$f_T = 0.331 D^{-1/6}\lambda^{-1}\left[\sec\zeta \int_0^\infty C_n^2(h) V_w^2(h)\, dh\right]^{1/2} \tag{13}$$

Here, f_T represents the tilt Greenwood frequency that describes the minimum closed-loop bandwidth required for tilt compensation, which tracks the changes in tilt due to turbulence in the continuously mixed air, depending on the state of atmospheric turbulence (Tyson 2000). The performance of the closed-loop bandwidth determines the adaptive optics performance for tilt based on how much faster it can move compared to the Greenwood frequency.

Finally, σ_{HO} arises from high-order aberrations in the wavefront. The wavefront distorted by turbulence includes not only tilt aberration but also all higher-order aberrations. σ_{HO} represents only the error resulting from the remaining high-order aberrations, excluding tilt aberration.

$$\sigma_{HO} = 0.129(\sigma_{tilt}) = 0.129\left(\sqrt{\langle \beta_a^2 \rangle}\right) \tag{14}$$

To correct the σ_{HO} term, the wavefront distortion caused by turbulence can be analyzed for high-order wavefront aberrations represented in Zernike polynomials using equipment such as Shack-Hartmann sensors. Compensation can be achieved by controlling a deformable mirror. However, we only focus on the effects caused by low-order (tip/tilt), and therefore, we do not consider high-order compensation.

In Table 2, both the uncompensated σ_{tilt} and the compensated σ_{tilt} for strong turbulence are presented.

The compensated σ_{tilt} for each zenith angle decreased approximately by 87% (86.9% in the weak turbulence and by 87.1% in the strong turbulence) compared to before compensation, and the remaining 13% of the compensated

Table 2. The standard deviation of AoA fluctuation before and after tip/tilt compensation

	Weak turbulence			Strong turbulence		
Zenith angle [deg]	0	30	60	0	30	60
Uncompensated [arcsec]	0.52	0.56	0.73	1.94	2.09	2.75
Compensated [arcsec]	0.07	0.07	0.09	0.25	0.27	0.36

AoA, angle-of-arrival.

σ_{tilt} appears to be dominated by uncompensated σ_{HO}. This suggests that to achieve more precise beam center correction, compensation of high-order aberrations is also necessary.

3. RESULTS

3.1 Collected Power on the Detector

For the convenience of calculation, in Section 2.4, we looked into a method of approximating the intensity of the beam reaching the detector as a Gaussian distribution. If, as shown in Fig. 5, the beam's center reaches a point r_a away from the center of the detector due to AoA fluctuation, the detector will only capture a portion of the beam. In this case, the collected power of the beam at the detector can be approximated as follows (Yang et al. 2014) :

$$
\begin{aligned}
P_d(r_a;z) &= \int_{-a}^{a}\int_{\xi}^{\xi} \frac{2}{\pi\omega_{st}^2} exp\left(-2\frac{(x-r_a)^2+y^2}{\omega_{st}^2}\right)dydx \\
\xi &= \sqrt{a^2-x^2} \\
&\approx A_0 \exp\left(-\frac{2r_a^2}{\omega_{eq}^2}\right) \\
A_0 &= [erf(v)]^2, \\
v &= \left(\sqrt{\pi}a\right)/\left(\sqrt{2}\omega_{st}\right), \\
\omega_{eq}^2 &= \omega_{st}^2 \frac{\sqrt{\pi}erf(v)}{2v\ \exp(-v^2)}
\end{aligned}
\tag{15}
$$

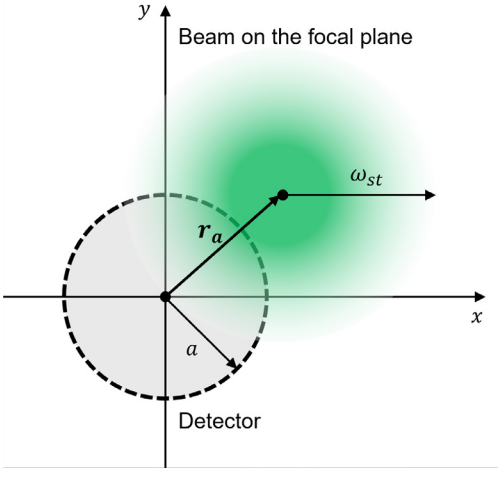

Fig. 5. The relationship between the beam reaching the focal plane and the detector area, where the gray area represents the detector's region and the green area represents the Gaussian distribution of the beam at the focal plane.

Here, A_0 is the fraction of collected power at r_a = 0 and ω_{eq} represents the equivalent beam width. The beam's size is determined by the intensity of turbulence. Depending on the beam's size, even if the beam's center reaches beyond the detector, power can still be detected. Conversely, when the beam arrives at the center of the detector (where the detectable power is maximum), any part of the beam extending beyond the detector's size will result in loss. Such loss cannot be compensated for by tip/tilt alone. In weak turbulence, nearly all of the beam is collected by the detector, while in strong turbulence, the collected beam is significantly reduced, as seen in Fig. 6.

In weak turbulence, since the size of the beam is smaller or similar to the size of the detector, the on-axis beam can be fully collected at the detector. Conversely, in strong turbulence, because the beam's size exceeds the detector's size, it is confirmed that a significant portion of the beam entering the detector can be lost even in the absence of pointing error.

Through simulations, we created 1,000 samples for each zenith angle, normalized the ratio of collected beams at the detector, and examined them. Additionally, we compared the collected beams at the detector under reduced tilt error achieved through tip/tilt mirror control. The comparison is presented in Fig. 7.

Tip/tilt compensation demonstrates a noticeable reduction in the fluctuation of the collected signal power at the detector. The upper limit of each fluctuation indicates the value of A_0, which is affected by the increased ω_{st} due to turbulence.

3.2 Probability Density Comparison between Non-Compensation and Compensation

The received power at the detector is determined by

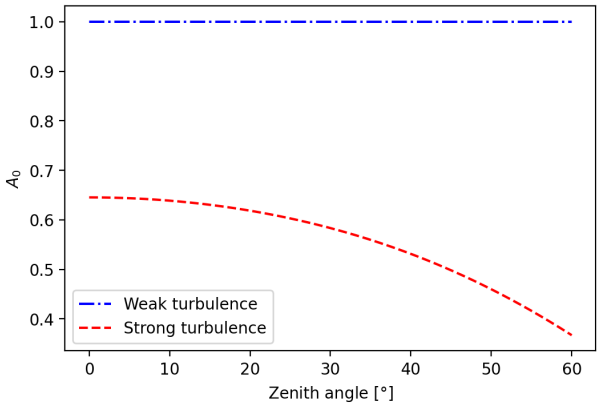

Fig. 6. Variation in the maximum fraction of collected power (A_0) that can be detected by the detector based on the zenith angle. The blue dashdotted line represents weak turbulence and the red dashed line represents strong turbulence.

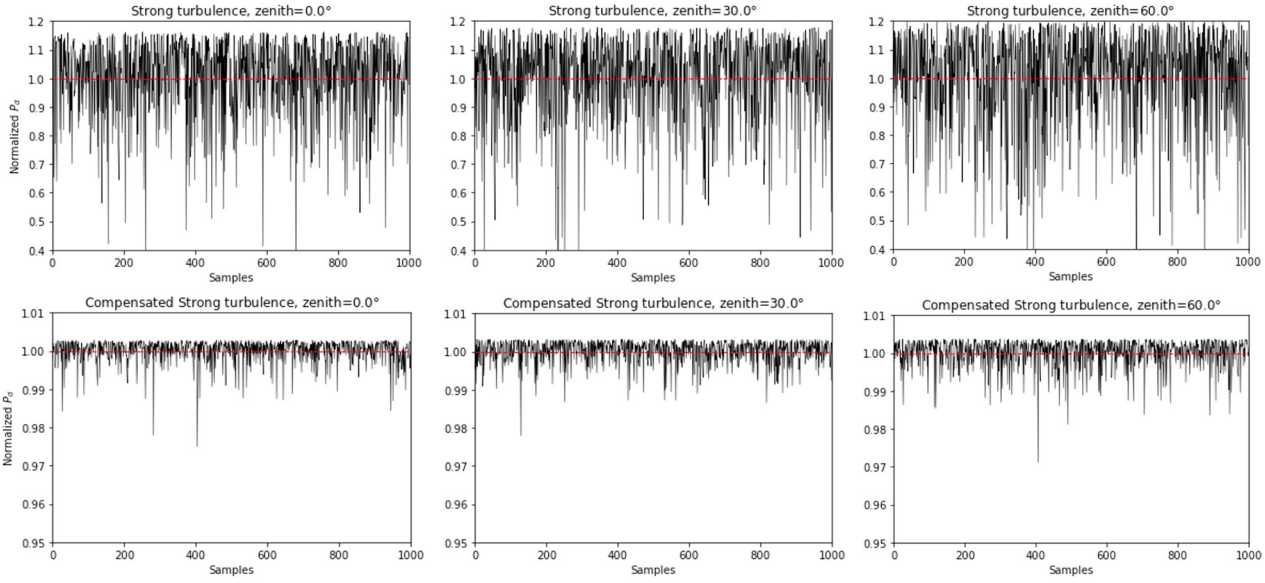

Fig. 7. The normalized power collected at the detector in strong turbulence. Simulation results before tip/tilt compensation (above) and after compensation (below).

the distance between the center of the detector and the center of the beam, r_a, as well as the beam size at the focal plane, ω_{st}. Moreover, the random distribution of r_a follows a Rayleigh distribution. The probability density function of the Rayleigh distribution is as follows:

$$p\left(r_a\right)=\frac{r_a}{\sigma_s^2}\cdot\exp\left[-\frac{r_a^2}{2\sigma_s^2}\right] \tag{16}$$

where, σ_s^2 is jitter variance at the receiver. The probability density function for the received power P_d at the detector is derived by combining Eqs. (15) and (16) (Farid & Hranilovic 2007).

$$p\left(P_d\right)=\frac{\gamma^2}{A_0^{\gamma^2}}P_d^{\gamma^2-1}$$
$$\gamma^2=\omega_{st}^2/4\sigma_s^2 \tag{17}$$

The collected power is normalized, and the power before and after tip/tilt compensation is compared. In the case of weak turbulence, it was confirmed that even without tip/tilt compensation, most of the beam profiles are already collectable within the detector region. The comparison results for strong turbulence are shown in Fig. 8.

In Fig. 8, the solid black line represents the Rayleigh probability density for normalized power, and the red star-shaped points indicate the distribution from simulated results of normalized power fluctuation. The probability density distribution also confirms that significant reduction in the loss of the collected signal beam at the detector can be achieved through tip/tilt compensation.

3.3 Bit Error Rate (BER) Comparison between Non-Compensation and Compensation

The performance of communication is quantified by the BER, which represents the ratio of error bits to the total transmitted bits. The BER depends not only on the modulation scheme used in communication but also on the received signal power. We have confirmed that tip/tilt compensation increases the probability of collecting power at the detector. This increase in received power for the beam can enhance the BER performance in communication systems using modulation schemes like on-off keying (OOK). The formula for calculating the average BER is as follows (Arpali et al. 2008):

$$\langle BER\rangle=\frac{1}{2}\int_0^\infty p\left(u\right)\cdot erfc\left(\frac{\langle SNR\rangle u}{2\sqrt{2}}\right)du \tag{18}$$

where p(u) is the probability density of normalized received power u and $erfc(\cdot)$ is the complementary error function.

As seen in Fig. 9, it is evident that tip/tilt compensation alone significantly improves the average BER. The uncompensated results show, as expected, that the lower the zenith angle is, the better the average BER is. The compensated results exhibit consistent improvement in

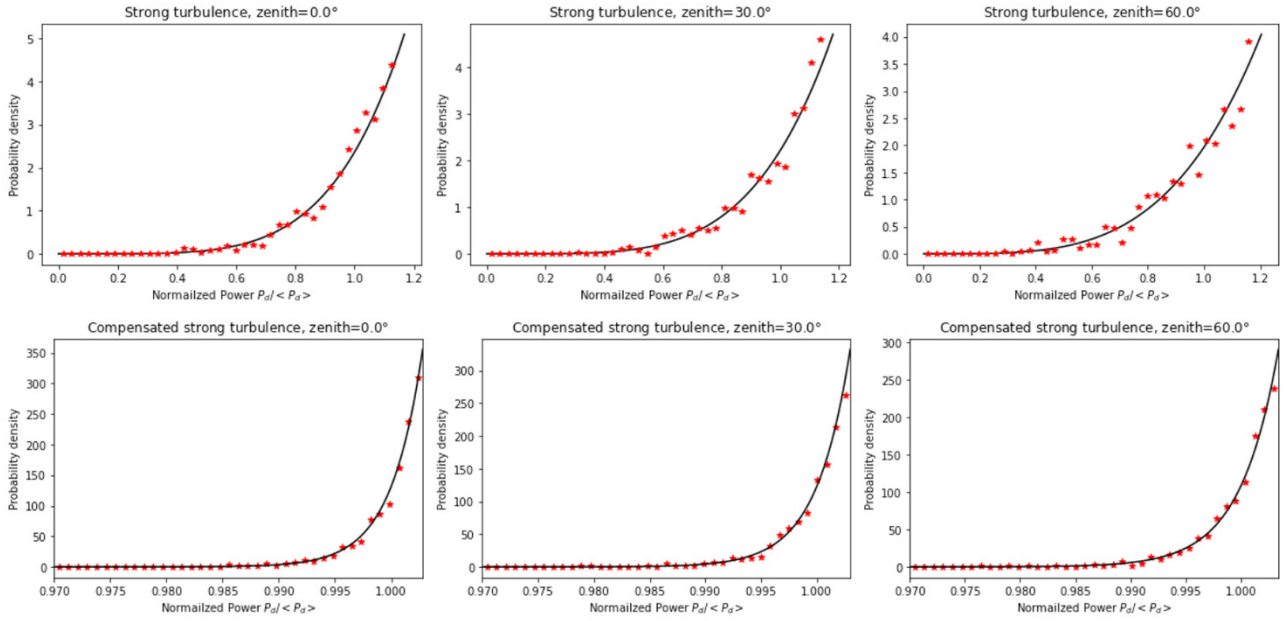

Fig. 8. Comparison of probability density before and after tip/tilt compensation.

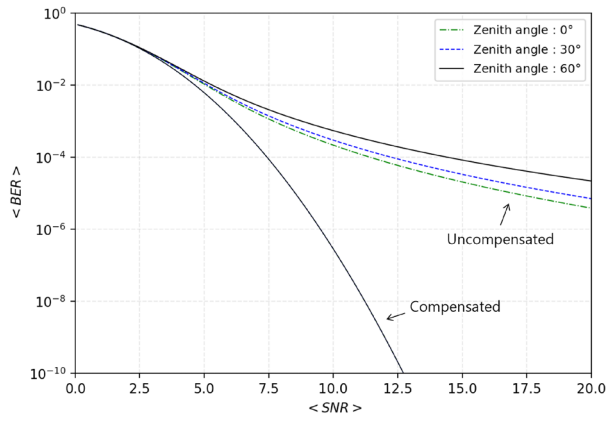

Fig. 9. Comparison of average BER before and after tip/tilt compensation. Green dashdotted line represents ζ = 0°, blue dashed line is ζ = 30°, and black solid line is ζ = 60°. BER, bit error rate.

terms of average BER regardless of zenith angle variations. This appears to be a limitation of tip/tilt compensation, and to achieve even better results, the correction of factors not considered in this study may be required.

4. SUMMARY AND DISCUSIONS

In this study, we analyzed the effect of tip/tilt compensation in terms of the intensity of atmospheric turbulence. Laser beams propagating through the Earth's atmosphere experience refraction due to atmospheric turbulence, resulting in AoA fluctuations at the receiver. This effect is more pronounced in the uplink scenario compared to the downlink. Furthermore, AoA fluctuations, along with the influence of receiver and transmitter jitter, contribute to image dancing on the focal plane. The effect of atmospheric turbulence was simulated for situations of weak turbulence and strong turbulence using the Hufnagel-Valley model, allowing us to estimate the displacement of beams on the focal plane. Additionally, we analyzed the variance of tip/tilt compensation, σ_{tilt}, to ascertain how effectively atmospheric turbulence can be compensated by using a tip/tilt mirror. It is shown that the tip/tilt compensation reduced significantly the tip/tilt error caused by atmospheric turbulence, approximately by 86.9% in the weak turbulence and by 87.1% in the strong turbulence. The remaining errors is analyzed to be resulted from the uncompensated terms of high-order aberrations in the wavefront.

Furthermore, we probabilistically calculated and simulated the power received by the detector both before and after tip/tilt compensation. We confirmed that the tip/tilt compensation increases the probability of power collected at the detector and also leads to improvements in the average BER.

We considered only the effect of beam wandering causing the AoA fluctuation to analyze the intensity variation affecting on the BER. But it is necessary to include the atmospheric attenuation and scintillation as well as high-order aberrations to analyze the performance of communication channel in the presence of atmospheric turbulence. The results obtained

from this study will be utilized in establishing the PAT system at the GEOL station, for the satellite-to-ground laser communication.

ACKNOWLEDGMENTS

This research was supported by the National Research Foundation of Korea (NRF) grant funded by the Korea government (MSIT) (NRF-2022R1A2C1092602).

ORCIDs

Seok-Min Song https://orcid.org/0000-0002-6451-4161
Hyung-Chul Lim https://orcid.org/0000-0001-5266-1335
Mansoo Choi https://orcid.org/0000-0003-2019-3615
Yu Yi https://orcid.org/0000-0001-9348-454X

REFERENCES

Abdelfatah R, Alshaer N, Ismail T, A review on pointing, acquisition, and tracking approaches in UAV-based fso communication systems, Opt. Quantum Electron. 54, 571 (2022). https://doi.org/10.1007/s11082-022-03968-2

Andrews LC, Field Guide to Atmospheric Optics (SPIE Press, Bellingham, 2019).

Andrews LC, Phillips RL, Laser Beam Propagation through Random Media (SPIE Press, Bellingham, 2005).

Arpali SA, Eyyuboğlu HT, Baykal Y, Bit error rates for general beams, Appl. Opt. 47, 5971-5975 (2008). https://doi.org/10.1364/AO.47.005971

Cheon Y, Muschinski A, Closed-form approximations for the angle-of-arrival variance of plane and spherical waves propagating through homogeneous and isotropic turbulence, J. Opt. Soc. Am. A 24, 415-422 (2007). https://doi.org/10.1364/JOSAA.24.000415

Farid AA, Hranilovic S, Outage capacity optimization for free-space optical links with pointing errors, J. Light. Technol. 25, 1702-1710 (2007). http://doi.org/10.1109/JLT.2007.899174

Fernandez V, Gómez-García J, Ocampos-Guillén A, Carrasco-Casado A, Correction of wavefront tilt caused by atmospheric turbulence using quadrant detectors for enabling fast free-space quantum communications in daylight, IEEE Access 6, 3336-3345 (2018). http://doi.org/10.1109/ACCESS.2018.2791099

Hemmati H, Near-earth Laser Communications (CRC press, New York, 2020).

Lim HC, Sung KP, Yu SY, Choi M, Park E, et al., Satellite laser ranging system at Geochang station, J. Astron. Space Sci. 35(4), 253-261 (2018). http://doi.org/10.5140/JASS.2018.35.4.253

Lim HC, Park JU, Choi M, Choi CS, Choi JD, et al., Performance analysis of DPSK optical communication for LEO-to-ground relay link via a GEO satellite, J. Astron. Space Sci. 37(1), 11-18 (2020a). https://doi.org/10.5140/JASS.2020.37.1.11

Lim HC, Yu SY, Sung KP, Park JU, Choi CS, et al., Performance analysis of M-ary optical communication over log-normal fading channels for CubeSat Platforms, J. Astron. Space Sci. 37(4), 219-228 (2020b). https://doi.org/10.5140/JASS.2020.37.4.219

Olivier SS, Max CE, Gavel DT, Brase JM, Tip-tilt compensation-resolution limits for ground-based telescopes using laser guide star adaptive optics, Astrophys. J. 407, 428-439 (1993). http://doi.org/10.1086/172525

Robbe S, Sorrente B, Cassaing F, Rabbia Y, Rousset G, Performance of the angle of arrival correction system of the I2T+ ASSI stellar interferometer, Astron. Astrophys. Suppl. Ser. 125, 367-380 (1997). http://doi.org/10.1051/aas:1997227

Shamsipour N, Mobashery A, Moradi M, Bit error rate reduction of optical communication by means of tip/tilt correction, Opt. Commun. 429, 152-157 (2018). https://doi.org/10.1016/j.optcom.2018.07.067

Tyson RK, Adaptive optics and ground-to-space laser communications, Appl. Opt. 35, 3640-3646 (1996). https://doi.org/10.1364/AO.35.003640

Tyson RK, Introduction to Adaptive Optics (SPIE Press, Bellingham, 2000).

Yang C, Jiang W, Rao C, Bit-error rate for free-space optical communication with tip–tilt compensation, Waves Random Complex Media 16, 281-292 (2006). https://doi.org/10.1080/17455030600791678

Yang F, Cheng J, Tsiftsis TA, Free-space optical communication with nonzero boresight pointing errors, IEEE Trans. Commun. 62, 713-725 (2014). http://doi.org/10.1109/TCOMM.2014.010914.130249